Supporting Online Material for

Late Archean Biospheric Oxygenation and Atmospheric Evolution

Alan J. Kaufman,* David T. Johnston, James Farquhar, Andrew L. Masterson, Timothy W. Lyons, Steve Bates, Ariel D. Anbar, Gail L. Arnold, Jessica Garvin, Roger Buick

*To whom correspondence should be addressed. E-mail: kaufman@geol.umd.edu

Published 28 September 2007, *Science* **317**, 1900 (2007)
DOI: 10.1126/science.1138700

This PDF file includes:

Supplemental Online Material for:

Late Archean biospheric oxygenation and atmospheric evolution

The Hamersley Core

The Hamersley core was recovered during the summer of 2004 as part of the Deep Time Drilling Project (DTDP) of the Astrobiology Drilling Program (ADP) of the NASA Astrobiology Institute (NAI). This project also involved the Geological Survey of Western Australia, Randolph Resources, Hamersley Iron, SIPA Resources International, and the University of Western Australia. This was one of ten cores recovered by the ADP in 2003–2004; seven others were collected as part of the Archean Biosphere Drilling Project (ABDP) (1), and two others were collected in collaboration between the DTDP and the ABDP. Therefore, this particular core is referred to as ABDP-9. The motivation for recovery of this specific core was to obtain materials free of modern contamination and weathering effects for biogeochemical analysis to characterize the nature of life and its environment in the late Archean, shortly before the rise of atmospheric oxygen.

Approximately 1000 m of continuous drill core spanning banded iron formation, kerogenous shales, basinal carbonates, shallower cherts and clastics, and meteorite impact horizons were recovered. The drill site was located at 21°59’29.5”S, 117°25’13.6”E, hole azimuth 186°, dip 89°, on the Pilbara craton of Western Australia (Figure S1). One half of the core is archived at the Geological Survey of Western Australia’s (GSWA) Perth Core Library. The other (working) half of the core is presently stored at the School of Earth and Space Exploration at Arizona State University. For more information about the DTDP or how to request samples, please see http://nai.nasa.gov/ADP/DTDP2004.cfm.

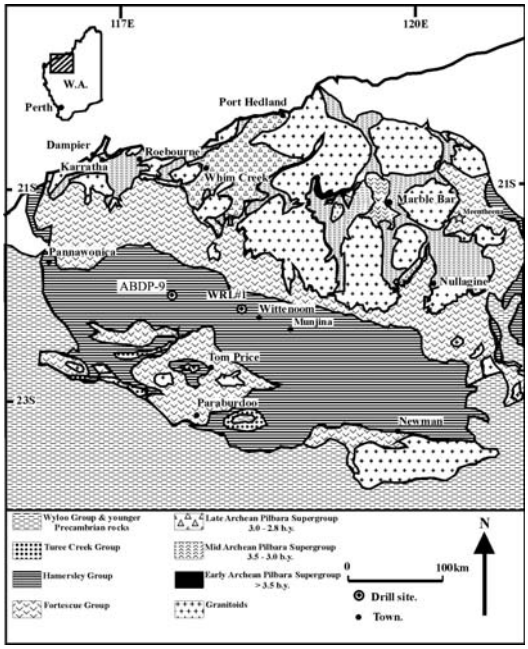

Figure S1: Simplified geologic map of the Pilbara Craton showing location of the ABDP-9 drill site.

Lithostratigraphy and sampling

The Mt. McRae Shale comprises approximately 85 meters of the upper part of the core. It is underlain by Mt. Sylvia Formation and capped by the Dales Gorge Member of the Brockman Iron Formation. The uppermost part is characterized by inter-bedded carbonates and grey/black shale with pyrite rarely to sparsely seen, gradually transiting into black shale with increasing pyrite content down section. Pyrite nodules occur massively from 131 m - 134 m followed by a 15 m thick section of black shale with frequent pyrite laminae and abundant pyrite nodules. Following this section, pyrite contents drops downcore as the lithology transitions to siderite banded iron formation (BIF). Continuing below 173 m depth, pyritic back shale becomes dominant again, with carbonate/marl interbeds, until the base of the Mt. McRae Shale. The core was sampled at 0.2 m ~ 2 m intervals for high-resolution analyses. For the purpose of this study sampling specifically avoided pyrite nodules. Laminae were avoided wherever possible. Where pyrite laminae were not avoidable (i.e., ~134 to 143 m) samples are labeled with a "pyl" suffix.

Bulk rock analyses

Powdered samples containing appreciable carbonate were sequentially acidified with 6M HCl, centrifuged and decanted. Residues were then washed with ultra-pure Milli-Q water, centrifuged, decanted, and dried overnight at 90^{o}C prior to elemental analyzer (EA) combustions. A Eurovector EA was used for on-line combustion of total sulfur in bulk powdered samples and the separation of SO on-line to a GV IsoPrime mass spectrometer for $^{34}S/^{32}S$ and $^{33}S/^{32}S$ analyses (2). The effluent from the EA is introduced in a flow of He (80-120 ml/min) to the IRMS through a SGE splitter valve that controls the variable open split. Timed pulses of SO reference gas (Air Products 99.9% purity, ~ 3nA) are introduced at the beginning of the run using an injector connected to the IRMS with a fixed open ratio split. The isotope ratios of reference and sample peaks are determined by monitoring ion beam intensities relative to background values.

Prepared samples (100-5,000 μgrams with equal amounts of V_2O_5) are accurately weighed and folded into small tin cups that are sequentially dropped with a pulsed O_2 purge of 12 ml into a catalytic combustion furnace operating at 1030^{o}C. The frosted quartz reaction tube is packed with reduced copper wire for quantitative oxidation and O_2 resorption. Water is removed from the combustion products with a 10-cm magnesium perchlorate column, and the SO is separated from other gases with a 0.8-m PTFE GC column packed with Porapak 50-80 mesh heated to 90^{o}C. The cycle time for these analyses was 420 seconds with reference gas injection as a 30-s pulse beginning at 20 seconds. Sample SO pulses begin at 150 seconds and return to baseline values between 200 and 250 seconds, depending on sample size and column conditions. Isotope ratios are determined by comparing integrated peak areas of m/z 48, 49, and 50 for the reference and sample SO pulses, relative to the baseline that is approximately 1 x 10^{-11}A. The background height is established from the left limit of the sample SO peak.

Standard notation

We use standard delta notation to represent isotopic compositions, where

$$\delta = 1000 * (R - 1).$$

For carbon,

$$R = \frac{\left(\frac{^{13}C}{^{12}C}\right)_{sample}}{\left(\frac{^{13}C}{^{12}C}\right)_{standard}}$$

whereas for sulfur

$$R = \frac{\left(\frac{^{3x}S}{^{32}S}\right)_{sample}}{\left(\frac{^{3x}S}{^{32}S}\right)_{standard}},$$

with x is either 3, 4 or 6. For ease of presentation and interpretation, we present ^{33}S and ^{36}S data as deviations (in ‰) from a reference fractionation line using capital delta notations:

$$\Delta^{33}S = \delta^{33}S - 1000 * ((1+\delta^{34}S/1000)^{0.515} - 1)$$

and

$$\Delta^{36}S = \delta^{36}S - 1000 * ((1+\delta^{34}S/1000)^{1.90} - 1).$$

The exponents in these expressions (0.515 and 1.9) are chosen to represent low temperature equilibrium (5).

Uncertainties of SO and SF_6 analyses

All bulk and residue samples were analyzed by the SO method in triplicate and reported values are averages of these measurements. Uncertainties (1σ) of triplicate analyses are better than 0.3‰ for both $\delta^{34}S$ and $\Delta^{33}S$ values, which is comparable with uncertainties based on multiple NBS-127 standard measurements (n ~ 15 to 20) during each analytical session.

For SF_6 analyses, Ag_2S samples were fluorinated under a ~10 X excess of F_2 at 250°C for 8 hours. The product SF_6 was cleaned via chromatographic and cryogenic techniques, and measured at m/z of 127-129 and 131 on a Thermo Finnigan MAT 253 gas source mass spectrometer. Uncertainties (1σ) on fluorination were determined based on long term reproducibility of international standards and are 0.14, 0.008, and 0.20‰ for $\delta^{34}S$, $\Delta^{33}S$, and $\Delta^{36}S$ respectively.

Comparison of SO and SF_6 measurements

While there is a high degree of stratigraphic coherence to the sulfur isotope compositions determined by the two techniques highlighted here, we also note differences outside of the demonstrated uncertainties in a subset of samples (Fig. S2).

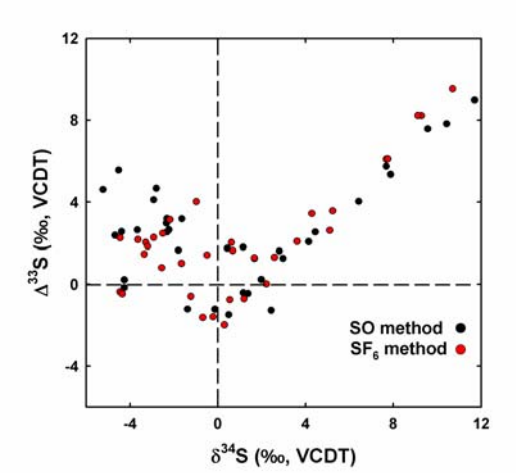

Figure S2: Comparison of $\delta^{34}S$ and $\Delta^{33}S$ of bulk powder from the Mt. McRae Shale analyzed by the SO method and extracted sulfides from the same samples by SF_6 techniques.

These are most pronounced in sulfur-poor carbonates from the top of the formation where SO values are notably enriched in ^{33}S relative to the SF_6 measurements of sulfides from the same samples. We attribute these offsets to interference either by excess CO_2 in the mass spectrometer source during SO ionization or to a difference in the sulfur that the SO technique and SF_6 techniques sample (i.e. trace sulfate in carbonate). On the other hand, small, but systematic differences in bulk rock and sulfide sulfur isotope compositions are also seen in some samples with abundant pyrite lower in the core. In this case, isolated sulfides are generally more enriched in ^{33}S, which makes it possible that either acid volatile sulfides – lost during the chemical isolation of pyrite sulfur – or organic-bound sulfur represent unaccounted and isotopically distinct reservoirs in these rocks warranting further research.

Sulfur isotope fractionations and geologic record:

The magnitudes of fractionations produced by mass-dependent processes are proportional to the relative masses of the isotopes involved and fit with theoretical predictions of equilibrium and kinetic isotope effects (see 3-7). A second class of geologically relevant isotopic fractionation processes has been called non mass-dependent (NMD) because they do not follow the traditional mass-dependent fractionation relationships, and it is inferred that factors other than mass contribute to these isotopic fractionations. This designation of NMD does not imply, however that mass terms are absent from the physics and chemistry that control these fractionation processes.

The observation of anomalous (NMD) sulfur isotope compositions in Archean and Paleoproterozoic rocks has been interpreted to reflect fundamental changes in the terrestrial sulfur cycle, in atmospheric chemistry, and in atmospheric oxygen content (Fig. S1; 8-18). The Archean record of large nonzero $\Delta^{33}S$ and $\Delta^{36}S$ values is thought to reflect an imprint of sulfur chemistry in an early atmosphere that was significantly less oxidizing and more transparent to ultraviolet light than the later atmosphere (8, 11, 19).

This data set significantly extends the range of observed late Archean NMD effects (Fig. S3).

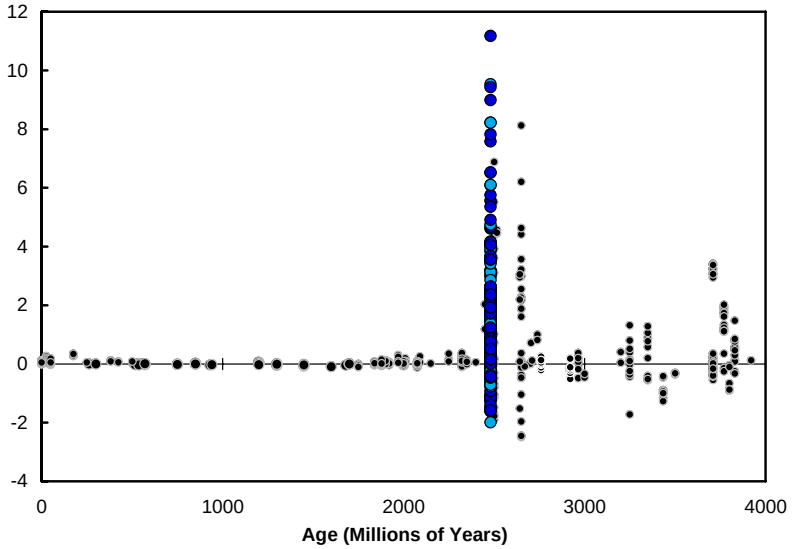

Figure S3: A compilation of $\Delta^{33}S$ versus time. This record has been subdivided into three stages. Stage 1 extends back from 2450 Ma and is marked by large NMD effects. Stage 2 is a transitional period from 2000-2450 Ma from a NMD record to the mass-dependent record of Stage 3 (< 2000 Ma). Light blue circles represent data from the ABDP-9 core (Hamersley Basin) whereas the dark blue circles are from the AD-5 core (Transvaal Basin). Published data in black are from 1, 8, 9, 13-18, 20-23.

A number of experimental and theoretical studies have been initiated in the last few years to find candidates for the source of the Archean isotope effects and a large number of these studies have focused on gas-phase chemistry. The present understanding of NMD isotope effects places their production largely with gas-phase reactions. The range of ultraviolet wavelengths investigated in previous studies (19, 24) is relevant to low oxygen atmospheres and are used as a basis for arguing that the chemistry is relevant as well.

Results from ABDP-9 in the Hamersley Basin, Western Australia

Samples analyzed for elemental and isotopic abundances from the ABDP-9 core and discussed in the text and illustrated in Figures 1 and 2 are reported in Table S1.

Results from AD-5 in the Transvaal Basin, South Africa

Stratigraphic trends in elemental and isotopic abundances of samples from the AD-5 core drilled near Pomfret, South Africa are reported in Figure S4 and Table S2. Total organic carbon, $\delta^{13}C$ of TOC, wt. % S, and a few $\delta^{34}S$ compositions were reported in (25). Most of these samples were poor in total sulfur and unsuitable for the bulk powder technique, so sulfide sulfur was chrome extracted from these and the results of SF_6 measurements are reported. Below the Tsineng Member of the Gamohaan Formation the coupled sulfur isotope composition, including the remarkable positive excursion near the base of the core, match those of the lower Mt. McRae Shale in Western Australia.

Samples from the Tsineng Member and the Kliphuis Member of the overlying Kuruman Iron Formation match sulfur isotope compositions with the upper Mt. McRae Shale.

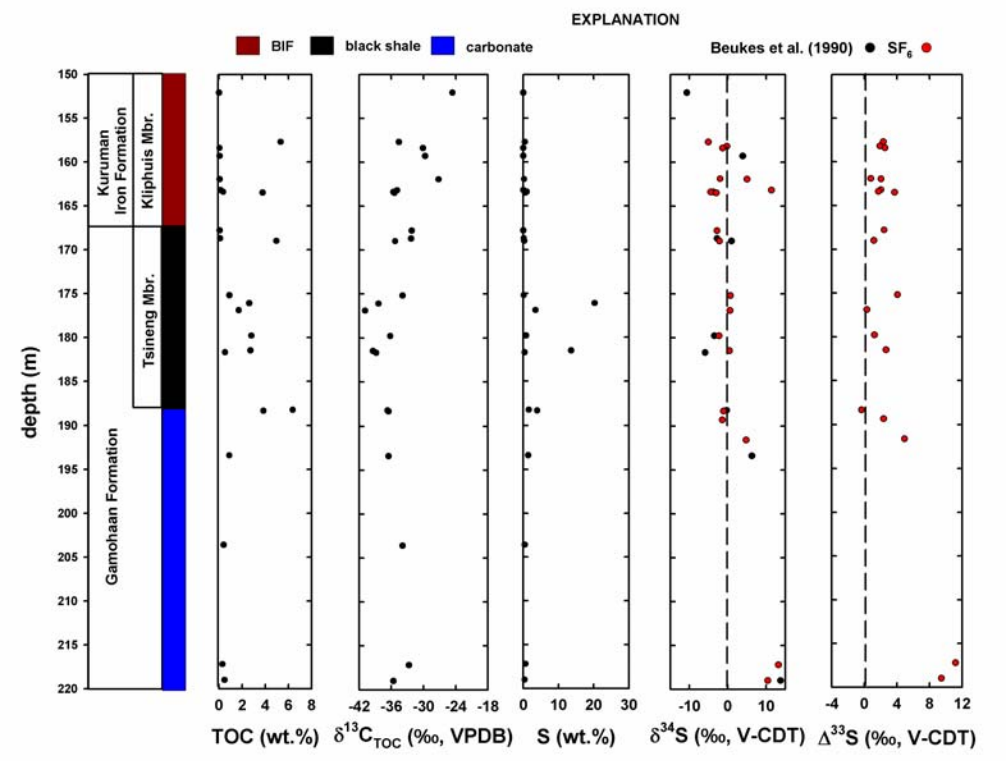

Figure S4: Time series elemental and isotopic trends in the ca. 2,500 Ma Campbellrand Formation and overlying Kuruman Iron Formation in South Africa from the AD-5 core. Trends in $\delta^{34}S$ and $\Delta^{33}S$ abundances in the lower and upper intervals match similar subdivisions in the Mt. McRae Shale in Western Australia.

We performed statistical analyses of the $\Delta^{36}S/\Delta^{33}S$ relationship for the South African sulfides, which correlate well (within 2σ) with sulfides from Western Australia and result in slope values of:

$$\text{(Upper units) } \Delta^{36}S = -1.5\ (\pm 0.2)\ \Delta^{33}S\ -0.4\ (\pm 0.3)$$

and

$$\text{(Lower units) } \Delta^{36}S = -0.87\ (\pm 0.08)\ \Delta^{33}S\ -0.4\ (\pm 0.4).$$

References:

1. H. Ohmoto *et al.*, Nature, **442**, 908 (2006).
2. K. A. Baublys, S. D. Golding, E. Young, B. S. Kamber, *Rapid Commun. Mass Spectrom.* **18**, 2765 (2004).
3. W. G. Mook, *UNESCO/IAEA* (2000).
4. E. D. Young, A. Galy, H. Nagahara, *Geochim. Cosmochim. Acta* **66**, 1095 (2002).
5. Y. Matsuhisa, J. R. Goldsmith, R. N. Clayton, *Geochim. Cosmochim. Acta* **42**, 173 (1978).
6. H. C. Urey, J. Chem. Soc., 562 (1947).
7. J. R. Hulston, H. G. Thode, *J. Geophys. Res.* **70**, 3475 (1965).
8. J. Farquhar, H.M. Bao, M. Thiemans, *Science* **289**, 756 (2000).
9. J. Farquhar et al., *Science* **298**, 2369 (2002).
10. B. Runnegar, C. D. Coath, J. R. Lyons, K. D. McKeegan, *Geochim. Cosmochim. Acta* **66**, A655 (Aug, 2002).
11. A. Pavlov, J. F. Kasting, *Astrobiology* **2**, 27 (2002).
12. B. A. Wing et al., *Geochim. Cosmochim. Acta* **66**, A840 (2002).
13. G. X. Hu, D. Rumble, P. L. Wang, *Geochim. Cosmochim. Acta* **67**, 3101 (2003).
14. S. J. Mojzsis, C. D. Coath, J. P. Greenwood, K. D. McKeegan, T. M. Harrison, *Geochim. Cosmochim. Acta* **67**, 1635 (2003).
15. S. Ono *et al.*, *Planet. Sci. Lett.* **213**, 15 (2003).
16. A. Bekker et al., *Nature* **427**, 117 (2004).
17. D. Papineau, S. J. Mojzsis, C. D. Coath, J. A. Karhu, K. D. McKeegan, *Geochim. Cosmochim. Acta* **69**, 5033 (2005).
18. M. J. Whitehouse, B. S. Kamber, C. M. Fedo, A. Lepland, *Chem. Geol.* 222, 112 (2005).
19. J. Farquhar, J. Savarino, S. Airieau, M. H. Thiemens, *J. Geophys. Res.* **106**, 32829 (2001).
20. S. Ono, B. Wing, D. Johnston, J. Farquhar, D. Rumble, *Geochim. Cosmochim. Acta* **70** (2006).
21 S. Ono, N. J. Beukes, D. Rumble, M. L. Fogel, *South African J. Geol.* **109**, 97 (2006).
22. D. T. Johnston et al., *Science* **310**, 1477 (Dec, 2005).
23. D. T. Johnston et al., *Geochim. Cosmochim. Acta* doi:10.1016/j.gca.2006.08.001.
24. B. A. Wing, J. R. Lyons, J. Farquhar, Geochimica Et Cosmochimica Acta 68, A781 (Jun, 2004).
25. N. J. Beukes, C. Klein, A. J. Kaufman, J. M. Hayes, *Econ. Geol.* **85**, 663 (1990).

Table S1: Results of mineralogic, elemental, and isotopic analyses of samples from the Mt. McRae Shale in the ABDP-9 drill core from Western Australia.

depth	% carbonate	$\delta^{13}C_{carb}$	$\delta^{18}O_{carb}$	% TOC	$\delta^{13}C_{TOC}$	% S_{SO}	$\delta^{33}S_{SO}$	$\delta^{34}S_{SO}$	$\Delta^{33}S_{SO}$	$\delta^{34}S_{SF6}$	$\Delta^{33}S_{SF6}$	$\Delta^{36}S_{SF6}$
105.65							-1.13	0.76	-1.52			
107.25		-8.22	-8.43							-6.09	0.625	0.08
108.27										-5.55	0.462	0.74
108.54		-8.06	-8.97							-2.40	0.979	-0.13
109.00	30.11	-3.12	-8.22	3.12	-34.96	1.21	-1.29	-0.13	-1.22	-0.17	-1.594	2.46
110.70	24.61			3.47	-33.27	0.51	0.92	-0.15	1.00			
111.00	45.99	-2.57	-6.85	2.74	-32.68	0.77	1.50	-2.23	2.65	-2.51	0.795	-0.55
111.76							-1.07	-2.04	-0.02			
112.52	38.84	-2.18	-6.78	3.66	-34.15	0.54	1.91	-5.23	4.61	-4.41	2.253	-2.32
113.46	16.30	-1.91	-6.55	5.84	-35.70	1.00	-0.03	-4.68	2.38	-3.60	2.164	-2.31
114.50	71.62	-1.83	-6.51	2.15	-35.48	0.65	4.17	0.04	4.16			
115.49	72.38	-1.92	-6.47	1.90	-35.48	0.20	0.75	-3.67	2.64	-3.24	2.034	-2.12
116.49	55.25	-2.19	-7.71	3.57	-34.04	0.51	2.00	-2.32	3.19	-2.88	2.269	-1.88
117.31	61.23	-2.43	-7.72	2.63	-33.44	0.34	2.34	-1.64	3.18	-2.14	3.135	-3.29
118.13						0.59	1.42	2.39	0.19			
119.24	63.15	-2.87	-7.43	2.90	-33.89	0.24	1.52	-1.68	2.39			
120.42	68.60	-2.26	-7.35	1.92	-33.10	0.17	2.60	-2.92	4.11	-0.94	4.009	-3.93
121.20	59.47	-2.08	-9.11	2.86	-34.62	0.27	1.36	-2.31	2.55	-2.46	2.468	-1.86
121.39	68.83	-1.68	-7.30	2.41	-34.11	0.40	1.78	-0.12	1.84			
122.32	46.50	-4.05	-9.06	3.73	-35.17	0.44	1.76	-2.34	2.97	-1.18	-0.598	0.64
123.22	61.30	-3.93	-7.80	2.29	-35.55		4.82	-3.29	6.51			
124.22	34.37	-3.72	-7.52	3.51	-35.27	0.30	3.22	-2.80	4.67	-1.61	1.007	-1.38
125.25		-4.84	-8.78			5.36	-1.96	-5.57	0.91			
126.15	23.95	-6.02	-9.99	4.11	-36.80	0.30	3.23	-4.52	5.56	-3.31	1.461	-0.42
127.25	18.03	-5.76	-9.61	6.91	-36.37	0.92	0.29	-4.39	2.56	-3.16	1.835	-1.59
128.17	14.21	-6.89	-10.65	6.50	-36.80	1.03	-0.67	-4.19	1.49			
129.01	12.08	-5.33	-10.92	6.14	-37.55	1.23	-1.91	-1.38	-1.21	-0.64	-1.625	1.53
130.06		-4.82	-10.60			0.66	-0.01	-0.83	0.42			

130.71	13.02	-4.82	-11.35	5.45	-36.08	5.37	0.72	-1.80	1.65	-0.45	1.414	-1.42
130.76	12.00	-4.61	-10.69	6.21	-36.74	0.35	-1.01	-3.15	0.62			
131.60	5.92			3.93	-39.53							
132.13	8.61			6.82	-38.63	0.54	0.50	0.63	0.18			
133.97	11.14			7.70	-41.36	0.63	0.58	0.97	0.08			
135.58	14.25	-4.96	-10.53	7.15	-41.29	14.29	2.40	1.15	1.81	0.66	2.025	-2.52
136.15	4.18			8.22	-41.46	3.93	-0.37	1.38	-1.08			
136.67	6.24			7.66	-40.70	5.28	0.46	1.89	-0.52			
136.94	13.59	-5.71	-10.81	9.02	-39.29	8.74	0.19	1.16	-0.41	0.59	-0.761	1.14
137.31						6.62	-0.48	0.34	-0.66			
137.68	5.72			9.41	-38.87	10.48	0.26	1.37	-0.45	1.23	-0.712	0.83
137.96	4.40			10.84	-39.51	6.25	-0.91	-1.51	-0.14			
138.38	6.67			10.86	-39.81	5.99	-1.40	-1.83	-0.46			
139.01	4.69			10.96	-40.23	11.55						
139.65	3.43			9.86	-40.49							
139.71	2.42			5.55	-39.79							
139.97	3.01			12.10	-40.54	5.42	-2.33	-4.25	-0.14			
140.25	3.33			12.43	-40.52	6.93						
140.50	9.29			15.34	-39.90	5.13	-1.98	-4.26	0.22	-4.42	-0.372	0.42
140.95	4.14			16.13	-40.06	6.32	-2.35	-4.26	-0.16	-4.31	-0.469	0.61
141.17	3.45			12.64	-40.26	6.59	-2.48	-2.41	-1.24			
141.47	7.36			13.03	-40.16	5.31						
142.08	3.85			11.65	-40.26	5.20	-1.17	-1.48	-0.41			
142.60						3.66	-1.37	0.25	-1.50			
143.45	9.62			13.07	-38.25	7.73	1.97	0.43	1.75	0.72	1.629	-1.42
144.36	17.99	-5.31	-10.84	8.72	-38.24	2.56	-0.77	0.65	-1.11			
145.61	13.45	-6.88	-11.66	13.41	-36.69	2.01	-1.78	-1.45	-1.03			
146.45	13.56	-7.96	-10.72	15.17	-36.71	5.73	-2.14	-1.89	-1.16			
147.30	10.07	-7.25	-11.47	12.60	-36.81	2.30	-0.38	1.41	-1.11			
148.27	8.91			10.45	-36.83	1.67	1.01	0.69	0.65			
149.30	9.78			12.09	-36.93	3.68	0.63	1.55	-0.17			
150.24	22.63	-5.03	-9.89	7.66	-36.97	2.23	3.00	2.56	1.69			
152.65	9.31			5.06	-38.30	1.00	2.71	2.97	1.18			
153.08	17.79	-3.90	-7.61	5.75	-39.87	1.49	5.62	4.16	3.48	4.27	3.417	-2.52

153.18	9.13			4.02	-37.86	0.60	-0.02	2.43	-1.27			
154.43	14.98			4.08	-38.35	2.47	-0.80	0.69	-1.15			
156.05	10.99			4.75	-38.58	0.34	0.18	1.06	-0.37			
157.80	24.32	-4.96	-8.22	4.32	-39.73	2.43	-1.22	0.50	-1.48	0.34	-1.986	1.99
158.91	15.92	-5.82	-9.00	4.84	-38.99	1.61	1.25	1.98	0.23	2.26	0.011	0.24
161.32	22.64	-6.34	-9.20	5.78	-39.02	1.56	2.79	2.97	1.26			
162.80	51.03	-6.73	-7.74	3.25	-38.70							
163.95	52.38	-7.32	-8.02	3.24	-39.33	2.16	3.47	3.31	1.77			
165.56	52.14	-6.81	-9.63	2.86	-38.51	0.82	3.78	2.27	2.62	2.65	2.508	-2.12
167.76	44.37	-7.52	-8.58	1.84	-37.52	0.49	2.12	1.67	1.26	1.71	1.289	-1.02
168.36	45.37	-7.85	-8.78	1.90	-37.79	0.90	3.05	2.80	1.61	2.62	1.306	-1.06
168.90	52.09	-7.62	-8.38	1.93	-37.60	2.44	9.39	7.87	5.35	7.73	6.089	-4.75
169.28	32.86	-7.95	-7.55	2.70	-38.49	1.50	1.88	2.89	0.39			
169.47	43.60	-7.84	-7.17	1.98	-38.56	9.10	12.50	9.56	7.58	9.32	8.217	-6.52
169.68	50.66	-8.50	-7.43	1.96	-38.18	1.54	3.82	3.19	2.18	2.67	1.920	-1.29
169.94	39.32	-7.73	-8.60	2.47	-38.23	3.49	13.17	10.43	7.82	9.15	8.221	-6.56
170.17	50.53	-8.24	-7.90	2.13	-38.10	2.43	7.33	6.42	4.03	5.28	3.562	-2.37
170.39	48.85	-8.39	-7.10	2.39	-40.12	3.10	9.69	7.67	5.75	7.79	6.103	-4.70
170.55	27.19	-8.65	-8.38	3.13	-38.16	2.62	4.20	4.14	2.07	3.66	2.080	-1.98
170.86	41.08	-8.66	-7.96	2.20	-38.45	1.84	6.71	5.58	3.84	5.40	3.905	-3.08
170.94	28.03	-8.69	-8.51	3.03	-38.80	5.39	15.00	11.70	8.99	10.74	9.533	-7.67
171.22	26.64	-8.50	-7.71	2.78	-38.63	3.24	7.36	6.19	4.17	5.99	4.752	-3.55
173.09	31.50	-9.75	-9.58	3.08	-38.48	1.71	0.39	0.95	-0.10			
173.50	36.35			2.69	-37.74	4.36	4.94	4.42	2.66	3.74	2.853	-2.38
173.73	42.00	-9.75	-9.90	2.79	-37.96	2.21	1.21	1.08	0.65			
174.67	33.03	-9.79	-8.92	2.92	-38.60	3.15	2.01	1.98	0.99			
175.51	23.77	-9.70	-8.19	3.82	-39.82	2.40	0.20	0.66	-0.14			
177.10	19.99	-9.50	-9.57	4.99	-41.12	3.00	-1.64	-2.30	-0.45	0.52	0.231	0.05
178.61	15.17	-8.69	-9.31	4.87	-39.94	3.48						
178.83	16.58			6.27	-41.60							
179.05	15.91	-9.00	-9.38	4.67	-39.60	3.09	-1.15	-0.76	-0.76			
180.33	19.85	-9.56	-9.27	5.01	-39.52	3.37	-0.88	-0.40	-0.67			
181.20	23.81	-9.80	-9.66	4.18	-39.27	2.66	-0.47	-0.44	-0.24			
182.50	14.07			4.37	-38.86	1.44	-0.31	0.12	-0.37			

183.65	22.15	-9.70	-9.26	3.11	-37.96	2.06	0.59	0.28	0.45			
185.43	34.06	-8.71	-9.59	2.50	-39.41	1.20	4.83	4.44	2.54	5.14	2.610	-2.17
187.46	13.69	-7.96	-9.67	3.55	-37.71	1.50	-0.02	0.57	-0.32			
188.01	17.10	-8.07	-9.80	3.98	-38.77	3.01	1.58	1.53	0.79			
188.87	22.67	-7.84	-9.93	3.32	-37.29	1.51						
189.39		-8.53	-9.99				2.49	2.40	1.26			

Table S2: Results of elemental and isotopic analyses of samples from the Campbellrand and Kuruman Iron formations in the AD-5 drill core from South Africa. % TOC, $\delta^{13}C_{TOC}$, % S, and $\delta^{34}S_{SO2}$ data from (25).

depth	% TOC	$\delta^{13}C_{TOC}$	% S	$\delta^{34}S_{SO2}$	$\delta^{34}S_{SF6}$	$\Delta^{33}S_{SF6}$	$\Delta^{36}S_{SF6}$
149.8							
152.1	0.01	-24.6	0.01	-10.7			
157.7	5.33	-34.6	0.46		-5.02	2.323	-3.51
158.2					-0.18	1.900	-2.41
158.4	0.05	-30.1	0.02		-1.26	2.520	-3.22
159.3	0.06	-29.7	0.04	3.9			
161.9					-1.94	0.770	-0.08
162.0	0.06	-27.2	0.23		5.08	2.037	-2.79
163.2	0.14	-34.9	0.03		11.46	2.026	-2.14
163.4	0.36	-35.6	0.99	-3.8	-4.39	1.714	-2.54
163.5	3.77	-35.4	0.53		-3.07	3.684	-4.76
167.8	0.07	-32.2	0.02		-2.76	2.410	-3.62
168.7	0.10	-32.3	0.15	-2.8			
169.0	4.95	-35.3	0.24	1.0	-2.11	1.152	-1.61
175.2	0.89	-33.9	0.15		0.75	4.060	-4.49
176.1	2.62	-38.4	20.28	21.0			
176.9	1.70	-40.9	3.49		0.62	0.288	0.95
178.9							
179.8	2.79	-36.2	0.81	-3.5	-2.26	1.240	-0.55
181.5	2.73	-39.4	13.62		0.52	2.644	-3.63
181.7	0.52	-38.8	0.4	-5.9	-6.30	1.924	-3.30

188.2	6.37	-36.7	1.55	-0.3	-0.41	0.152	0.73
188.3	3.84	-36.5	3.96		-0.99	-0.419	1.26
189.3					-1.36	2.368	-3.36
191.6					4.86	4.908	-4.12
193.4	0.89	-36.5	1.41	6.3	3.35	3.547	-2.24
203.6	0.41	-33.9	0.44		5.71	0.516	0.79
217.2	0.30	-32.7	0.63		13.26	11.177	-8.50
219.0	0.49	-35.6	0.41	13.8	10.48	9.428	-8.01